Subproject F 3.04

Printable Batteries

Principle Investigators: Sylvio Indris, Norman Mechau and Horst Hahn

CFN-Financed Scientists: H. Vasilchina (3/4 BAT IIa, 4 months), M. Kaus (3/4 BAT IIa, 7 months)

Institut für Nanotechnologie
Karlsruher Institut für Technologie

1 Introduction and Summary

Printable electronic circuits offer the possibility to produce ultra-thin and flexible electronics for mass applications. Many of the anticipated applications require a power source, for example for the implementation of a display. In order to use the same processing technology, a printable battery is desirable. Lithium ion batteries, that are currently used in portable electronic devices such as notebooks, mobile phones and digital cameras, have a high energy and power density and are the device of choice also for this application.

In this project, we developed a new concept for the production of ultra-thin Li-ion batteries on flexible substrates, by printing the electrode materials directly on top of the substrate. Pushparaj et al. showed that paper can be used as separator and support for the electrolyte in Li-ion batteries by impregnating films of carbon nanotubes with cellulose. [1] As electrolytes ionic liquids, KOH, and solutions of $LiPF_6$ were used. Additionally, human body liquids, like blood and sweat, were tested, which would enable possibly the implantation of batteries. As negative electrode materials, we will use nanoparticles of metal oxide, such as ZnO, in combination with amorphous carbon. Films of these metal oxides have been prepared by printing techniques and have a high specific charge capacity [2-4]. Furthermore, for the next step we will use nanocrystalline $LiFePO_4$ und $Li_4Ti_5O_{12}$, that have not been prepared by printing processes yet, as positive electrodes. These materials are studied extensively with respect to applications in conventional Li ion batteries and are already used commercially [5, 6].

In future applications, the printable battery production process has the potential to be integrated into the production of the complete active devices. The advantage of printing batteries is obvious: the electrodes can be structured in a rapid and simple way, enabling the combination of different electrode materials for hybrid battery systems that include components with high energy density as well as components with high power density. For applications in mass markets the processes are very cost effective [7-9]. Furthermore, the combination of printable batteries with solar cells, i.e. the concept of storing electric energy directly at the site of the energy conversion, gives an alternative to feeding the renewable energy into the electric grid.

The first part of this project belongs to the preparation and stabilization of suitable dispersions of the metal oxides for the printing process. The nanomaterials and the morphology of the printed films was investigated by using X-ray diffraction (XRD), scanning electron microscopy (SEM), transmission electron microscopy (TEM), and atomic-force microscopy (AFM). Subsequently, the dispersions were processed on flexible paper by ink-jet-printing process or spin coating. The battery performance of the samples was tested in Swagelok type batteries. From the galvanostatic cycling we got the information about the specific charge capacity, energy density, power density and cycle lifetime.

2 Material:

2.1 Model system- nanocrystalline Zinc Oxide (ZnO)

Nanoparticulate ZnO was used as a model system. In the experiments we used different powders of commercially available ZnO nano particles from Alfa Aesar and Evonik. The particles were different in size and shape. The size distribution of each batch was measured by SEM image and counting, cf. Fig. 1. The size of the particles ranges from 20 nm to several 100 nm. The sample with the smallest particles, shown in in Fig. 1 a), is BatchNr 44533 from Alfa Aesar. These particles have a narrow size distribution, the average diameter is 20 nm, and the shape of particles is spherical. In Figure 2b, ZnO AdNano from Evonik, the particle sizes are distributed between 20 nm and 100 nm. The shape of the particles shows strong variations, with spherical- as well as rod-like particles. The particles sizes from Batch Nr 44898, Fig. 1 c), are distributed between 40 and

200 nm. The shape is generally rod-like . The particles in Figure 1d, BatchNr 44299, are flat and flake-like. All the results are summarized in Table 1.

Table1:

BatchNr	Supplier	Size	Shape	Figure 1
44533	Alfa Aesar	20 nm	Spherical Particles	a)
ZnO AdNano	Evonik	20 – 100 nm	Particles, Rods	b)
44898	Alfa Aesar	40- 250 nm	Particles, Rods	c)
44299	Alfa Aesar	50- 450 nm	Flakes	d)

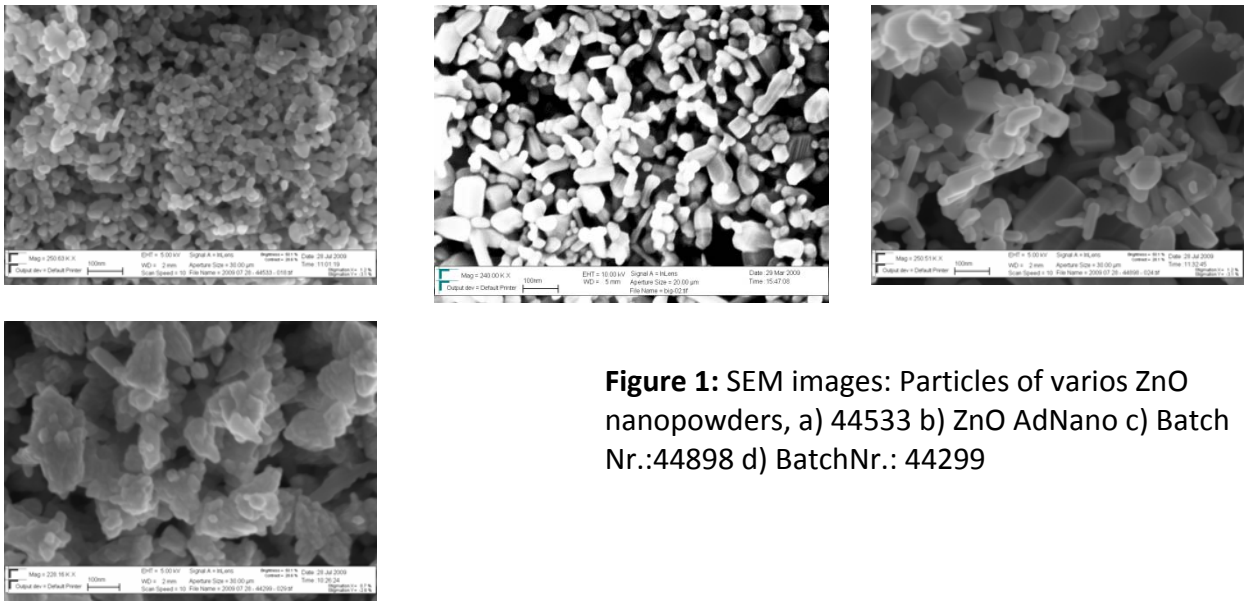

Figure 1: SEM images: Particles of varios ZnO nanopowders, a) 44533 b) ZnO AdNano c) Batch Nr.:44898 d) BatchNr.: 44299

The size and the shape of the particles show broad distributions, with particle sizes between 20 nm and 200 nm. Nevertheless, all the particles are crystalline. The XRD patterns are shown in Figure 2. From the width of the peaks the crystallite size was calculated. The crystallite size is about 18 nm for the samples from Alfa Aesar and about 30 nm for the samples from Evonik.

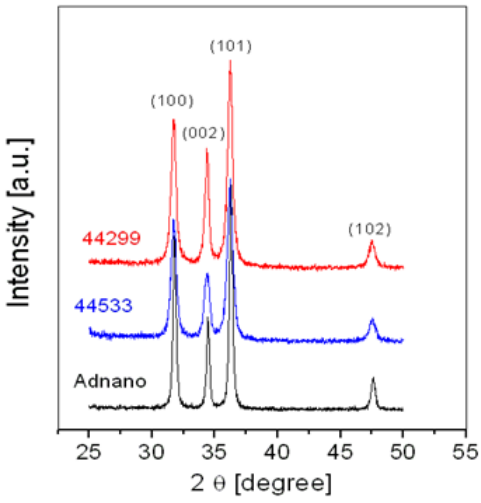

ZnO	Crystallite size [nm] (100 peak)	Crystallite size [nm] (101 peak)
44299	18.36	18.99
44533	17.99	17.83
Adnano	29.78	29.13

Figure 2: XRD patterns of the different ZnO nanopowders.

This reveals that the bigger particles are agglomerates of smaller crystals of 20 nm in size. This agglomeration takes place during the gas phase process. The size of the particles is important, because the morphology of the layers is strongly affected by the size and the distribution of the particles. Bigger particles include more voids, less density and the layers are more porous.

2.2 Dispersion and stabilization of nanoparticulate ZnO

For a solution process like ink-jet printing and spin coating the material has to be dispersed in a solvent. However, particles in a solution tend to agglomerate resulting in instable dispersions. To reduce the agglomeration of the particles in the solution the particles have to be stabilized. The stabilization of particles depends on many parameters, e.g. the size, the surface conditions, the stabilizer molecules, and the solvent. In all experiments the solvent and the stabilizer molecule was fixed. We used 2-Methoxyethanol as solvent and a commercial co-polymeric (Tego 751) as stabilizer. The dispersion was processed by a homemade dispersing process. After dispersing the size of the particles within the dispersion was measured by dynamic light scattering (DLS). The results are summarized in Table 2. The particle sizes in the solution are much bigger compared to the values of the dry powder. This is due to further agglomeration of the particles in the solution. The stabilization against agglomeration is not sufficiently effective for all particles. The results show that the smallest particles create the biggest agglomerates, although no clear correlation between powder particle size and the agglomeration in the solution can be observed.

Table 2:

BatchNr	**Powder particle size**	**Agglomerate size in solution**
44533	20 nm	400 – 2000 nm
ZnO AdNano	20 – 100 nm	80 – 400 nm
44898	40- 250 nm	400 – 500 nm
44299	50- 450 nm	80 – 800 nm

In addition to the size of the particles the surface modification and the surface condition are important for stabilization. This is due to the interaction between the surface defects in ZnO and the stabilizer molecules. Higher concentration of surface defects will enhance the stabilization. Surface defects in ZnO are well studied by photoluminescence.[10] In Fig. 3 the photoluminescence spectra of the particles are shown. The spectra show a characteristic peak at 390 nm and a second peaks at higher wavelengths between 400 nm and 800 nm. The peak π^* at 640 nm is an artifact from the system, the second order of the excitation wavelengths at 320 nm. The peak at 390 nm belongs to the excitation recombination within the bulk material. The second broad peak between 400 nm and 800 nm belongs to defect states at the surface. The change in the position is due to the energy distribution of the defects. The concentration of defects is proportional to the photoluminescence intensity.

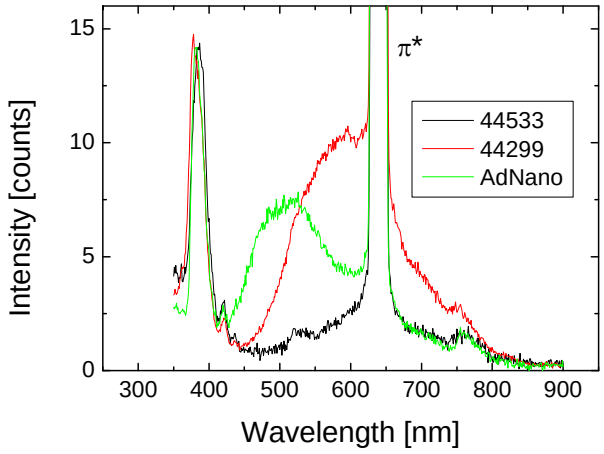

Figure 3:
Photoluminescence spectra of different ZnO nano particles in a solution of 2-Methoxyethanol. Two different peaks can be observed: a fixed peak at 385 nm for all particles and peaks at longer wavelengths. The peaks are due to the excitation recombination of the bulk material at 385 nm and recombination from surface states at longer wavelength. The peak π* is the second order of the excitation wavelength at 320 nm.

The lowest intensity is given for batch Nr 44533. The low intensity is due to a low concentration of defect states with a low defect state concentration belonging to stronger agglomeration. The sizes of the agglomerates are in the range from 400 nm to 2 µm. These sizes are too big for ink-jet printing, because the clogging of nozzles is one of the main problems in ink-jet printing. From practical point of view the particles have to be 100 times smaller compared to the nozzle size. The nozzle size in all the experiments was 24 µm, so particles smaller than 240 nm are necessary.

3. Ink-Jet Printing

Inkjet printing is an established technology in color document production. [11] The advantage of this technology is the flexibility in structuring in combination with high throughput. In all experiments we use the material printer Dimatix DMP-2800. We used a stabilized ink of ZnO nano–particles dispersed in water. For ink-jet printing we changed the solvent from 2-Methoxyethanol to water because of the safely regulations. Printing of water is difficult compared to 2-Methoxyethanol because of the high surface tension of the water. The droplet formation for the ink-jet process depends on fluid parameters and technical parameters. The fluid parameters can be summarized in the dimensionsless inverse Ohnesorge number- Oh^{-1}

$$Oh^{-1} = \frac{\sqrt{d \cdot \rho \cdot \gamma}}{\eta}$$

where d is the diameter of the nozzle aperture (24 µm), ρ are the density, γ is the surface tension and η is the dynamic viscosity of the ink. A droplet formation is only possible for inverse Ohnesorge number in the range $1 < OH^{-1} < 10$. [12] For the ink we measured the dynamic viscosity, the surface tension and the density of the ink; summarized in Table 3. For the inverse "Ohnesorge number" we obtained $Oh^{-1} = 9.89$

Table 3:

	Viscosity	Surface tension	Density
ZnO Ink	2,3 mPa	32 nN/m	1.3 g/cm^3

Technical parameters are the piezoelectric voltage and the wave function. The wave function actuates the piezoelectric. Both parameters were optimized for the process. The droplet

formation of an ink is shown in Figure 4. The firing voltage was 23 V. The aim is to get one droplet without any so-called “satellites”, i.e. additional smaller droplets.

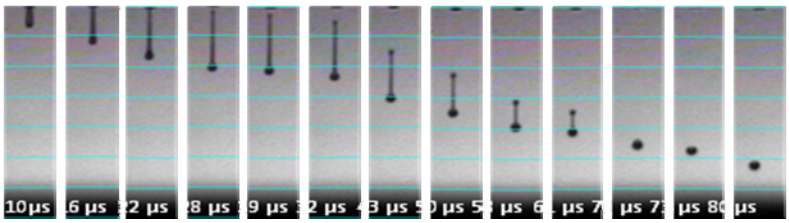

Figure 4:
Drop formation of stabilized ZnO ink dispersed in water.

In addition to the fluid parameters we optimized the size of the particles to reduce the clogging of the nozzles. After the dispersing process the particles are distributed in size from 40 nm to 400 nm for the batch AdNano. To further reduce the agglomerate size we used a centrifugation step. After centrifugation the particle sizes are reduced to less than 200 nm and for this case no agglomeration was observed.

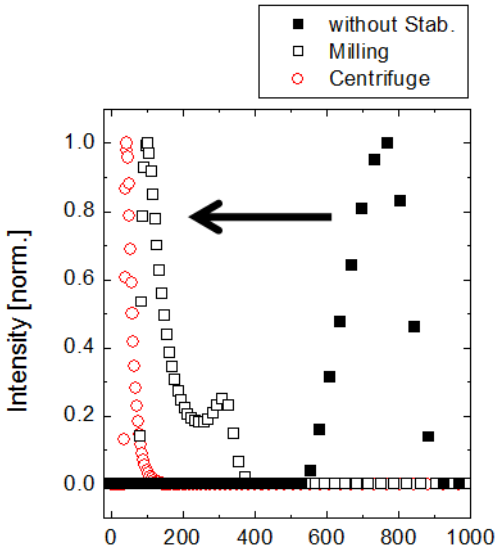

Figure 5:
Dynamic light scattering on ZnO dispersions after different processing steps. The size of agglomerated particles is reduced by stabilization of nano particles within the solution.

4. Battery performance

The different ZnO powders were tested in two-electrode coin cells against Li metal counter electrodes. Galvanostatic cycling was performed in the voltage window 0.02 V-3V. We used a rate of C/100, i.e. complete discharge/charge within 100 h, and 1M $LiPF_6$ in EC/DMC as electrolyte. The results are shown in Fig. 5. The first discharge is characterized by a long, flat plateau at about 0.6 V. Its length corresponds to a large specific capacity of about 1000 mAh/g. This corresponds to insertion of about 3 Li ions per formula unit ZnO and thus is consistent with the mechanism described by the subsequent reactions:

$$2Li + ZnO \rightarrow Li_2O + Zn$$
$$Li + Zn \rightarrow LiZn.$$

In the following charging/discharging steps strong decreases of the specific capacity are observed. This has to be attributed to the formation of new phases coming along with big volume changes

(especially during the LiZn alloy formation), separation of the discharging products and thus very limited reversibility of the above described reactions. We could show that the capacity retention is best for the electrodes with the smallest particle sizes.

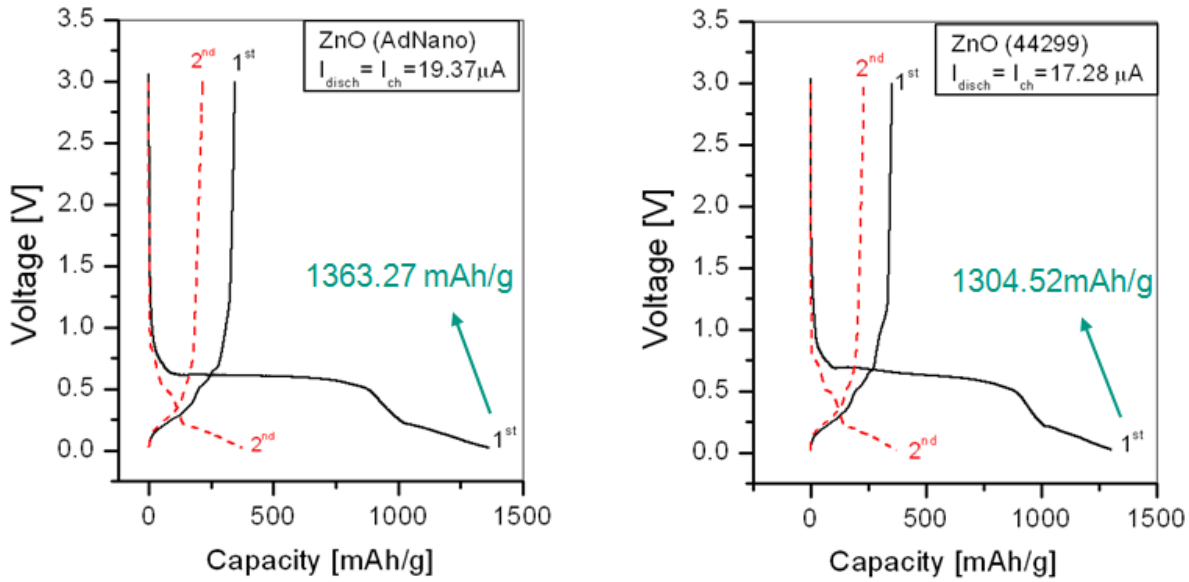

Figure. 6: The voltage profiles during galvanostatic charging/discharging for two different printed ZnO electrodes.

References

[1] V. L. Pushparaj, M. M. Shaijumon, A. Kumar, S. Murugesan, L. Ci, R. Vajtai, R. J. Linhardt, O. Namalesku, and P. M. Ajayan, *Proc. Natl. Acad. Sci. USA* **104**, 13574-13577 (2007).
[2] Y.-Y Noh, X. Cheng, H. Sirringhaus, J. Sohn, M. Welland, D. Kang, *Appl. Phys. Lett.* **91**, 043109 (2007).
[3] J. R. Dahn, T. Zheng, Y. Liu, and J. S. Xue, Science **270**, 590-593 (1995).
[4] A. Courtney and J. R. Dahn, *J. Electrochem. Soc.* **144**, 2045-2052 (1997).
[5] A. Yamada, S. C. Chung, and K. Hinokuma, *J. Electrochem. Soc.* **147**, A224-A229 (2001).
[6] L. Cheng, X.-L. Li, H.-J. Liu, H.-M. Xiong, P.-W. Zhang, and Y.-Y. Xia, *J. Electrochem. Soc.* **154**, A692-A697 (2007).
[7] E. Menard, M. Meitl, Y. Sun, J. Park, D. Shir, Y. Nam, S. Jeon, J. Rogers, *Chem.Rev.* **107**, 1117-1160 (2007).
[8] P. Calvert, *Chem. Mater* **13**, 3299-3305, (2001).
[9] T. Kraus, L. Malaquin, W. Riess, N. D. Spencer, H. Wolf, *Nature Nanotechnology* **2**, 570-576 (2007).
[10] A. B. Djurisic and Y. H. Leung, Small **2**, 944- 961 (2006).
[11] H. Wijshoff, Physics Reports-Review Section of Physics Letters **491,** 77-177 (2010).
[12] E. Tekin, P. J. Schmith and U. Schubert, Soft Matter **4**, 703- 713 (2008).